

Embedded metallic nanopatterns for enhanced optical absorption

Fan Ye, Michael J. Burns, Michael J. Naughton*

Department of Physics, Boston College, Chestnut Hill MA 02467

ABSTRACT

Novel metallic nanopatterns integrated with semiconductor films form optical metamaterials that can enable enhanced absorption. When employed in photovoltaics, such integrated nanostructures may facilitate significant increases in power conversion efficiency. Here, we show that metal nanopatterns embedded within a semiconductor, as opposed to being situated at/on the surface(s), exhibit absorbance enhancements that exceed those yielded by surface patterns. We show in computer simulations and experiments that absorbance in amorphous silicon can be enhanced many-fold for embedded metal nanopatterns (EMN) in ultrathin silicon films in particular wavelength regimes. Compared to plane *a*-Si films of comparable thickness, a several hundred percent enhancement is observed. This represents a potential route to high efficiency solar power with ultrathin absorbers enhanced by EMN-based optical metamedia.

Keywords: Metamaterials, photovoltaics, nanopatterns, simulations, embedded structures

1. INTRODUCTION

There is significant effort, worldwide and across all thin-film PV materials systems, aimed at increasing light absorption in photovoltaic (PV) layers of thin-film solar cells while simultaneously making the PV layer itself thinner to enable more efficient carrier extraction and reduced material consumption. A number of innovative architectural approaches, such as nanocoax and nanowire configurations, as well as nanoantennas and metamaterials have been applied to thin-film solar cells with this in mind. In the case of metamaterials, metal films have been overlaid on the PV absorber and patterned on scales much smaller than the wavelength of light in such a way as to enhance the total absorption of the system, by increasing forward scattering, perhaps aided by plasmonic effects. Similarly, subwavelength nanoparticles/patterns can be used as novel back-reflectors potentially leading to enhanced optical absorption in the PV layer. Computer simulations show that the presence of such subwavelength metal patterns can induce electromagnetic field enhancement in the vicinity of the metal. [1,2] Experiments using Au [3] or Au core-shell [4] nanoparticles dispersed atop an ITO film on a *p-i-n a*-Si solar cell were shown to improve PV performance by ~10% as a result of enhanced forward scattering from surface plasmon polaritons in the vicinity of the nanoparticles. Metal nanoparticles used at front- and back-side scatterers in silicon solar cells have been reported to qualitatively reduce reflection and increase photocurrent or short circuit current density J_{sc} . [5,6] In another experiment, Ag nanoparticles were placed on a Ag substrate and coated with an ITO film, followed by *n-i-p a*-Si. [7] These authors observed a 20% increase in photogenerated current compared to controls without the nanoparticles, attributed to localized surface plasmons. This current gain was reportedly accompanied by a 20% decrease in solar cell fill factor, such that there was apparently no power conversion efficiency improvement, though the fill factor issue could be related to variations in the *a*-Si growth mechanism caused by the presence of the nanoparticles, which can presumably be addressed. Differing from both of the top/bottom surface approaches are tactics that share some similarity to that employed here, though there are important differences. In Ref. [8], dielectric rather than metallic nanoparticles were embedded directly within the absorbing medium, as a mechanism for enhancing lateral scattering and thus optical absorption. Up to a 10% increase in integrated absorption was simulated. In Ref. [9], Ag nanoclusters were embedded in the absorber layer of an organic heterojunction solar cell, and a 15% increase in J_{sc} was observed and attributed to plasmonic effects.

Approaches that employ metal nanopatterns/particles as front or back scatterers only capitalize on a portion of the concentrated electromagnetic field around the metal patterns. Meanwhile, embedded dielectric nanoparticles are rather weak scatterers of optical electromagnetism. Embedding a metal pattern entirely within the PV layer of the solar cell, however, can allow one to exploit the strong scattering from subwavelength metal nanostructures as well as potentially harvest all of the scattered light by the embedded metal nanopattern (EMN), and thus to increase the number of photo-

*naughton@bc.edu; phone 1 617 552-0635

generated electron-hole pairs. In this work, we study by simulation and experiment the optical absorption of ultra-thin *a*-Si-EMN composite structures where the structured metallic metamaterial patterns are embedded within the PV film.

2. SIMULATIONS

Simulations were performed on an 8-core CPU PC with a 448-core GPU using CST Microwave Studio. Simulations for two different nanopatterns embedded at various depths in thin *a*-Si films were performed in the time domain using the finite integration technique (FIT). Full dispersion relations, obtained from ellipsometry in our lab for *a*-Si, and from standard literature sources for the metals [10], were employed in all simulations.

2.1 Alternating Square EMN on ITO-Glass

The unit cell of the first pattern is 400 nm on a side, with the metal pattern consisted of 200 nm metal squares in an alternating square pattern, as illustrated in Figure 1, with the plane of the structure aligned to the *x* & *y* axes of the coordinate system and the *z*-axis normal to the plane of the pattern. The simulation consisted of placing periodic boundary conditions on the unit cell in the *x* & *y* directions, and simulating a plane wave impacting the system along the *z* direction. The reflection and transmission of the incident plane wave normal to the *z*-axis were simulated, thus simulating 0th order reflection *R* and transmission *T*, yielding absorbance/absorption *A* via $A = 1 - R - T$.

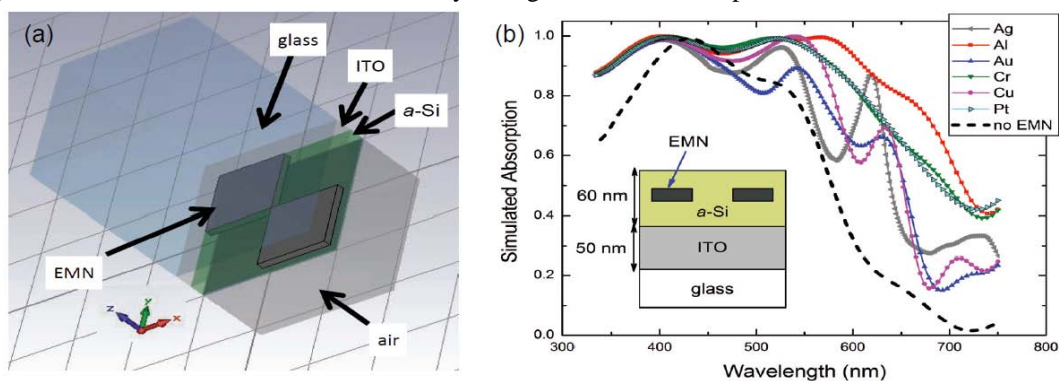


Figure 1. (a) Illustration of the 400 nm x 400 nm unit cell for simulations of an infinite array of metallic squares embedded in an *a*-Si absorber layer in an alternating square pattern (EMN). (b) Simulated optical absorbance of the structure for various metals, for light incident from the glass side. Similar results are obtained for light incident from the vacuum side. The simulated layer thicknesses were: 50 nm ITO, 60 nm *a*-Si, 500 nm glass, 20 nm EMN, with the EMN embedded by a distance of 25 nm into the *a*-Si below the glass surface. Note that even this simple EMN structure has a noticeable effect on the absorption spectrum of the system, especially at the longer wavelengths.

We found that the choice of metal and the details of its shape and placement affect the absorption of light in these structures. In Figure 1(a) we show a schematic of the alternating square EMN structure and in Figure 1(b) absorption simulations for this structure where only the metals were changed. In these simulations, the full dispersion relations of all of the materials were used, thus illustrating how sensitive the systems are to the detailed material properties of the constituents. Also shown for comparison is a film of *a*-Si with the same thickness as that used in the EMN absorption simulations. It can be seen that, for all metals employed, inclusion of the EMN significantly increases optical absorption, especially at longer wavelengths. Some issues to be addressed in next steps relate to precisely where the optical energy being absorbed (*i.e.* in the *a*-Si, or in the EMN), and the role, if any, that plasmonics play in these structures and results. A hint with regard to the latter is given by Figure 1(b), where it can be seen that the best simulated absorption occurs with an aluminum EMN, followed by chromium and platinum, with the smallest enhancements occurring in copper, gold and silver. Note that the metals in this latter group all have smaller plasma frequencies than those in the former,¹¹ which are deeper in the UV. Moreover, Cu, Ag, etc. have interband transitions at visible wavelengths and are known to absorb electromagnetic energy there. Nonetheless, EMNs with the “non-plasmonic” metals are more highly absorptive, suggesting that the EMN structure plays a larger role than the excitation of surface plasmon modes in defining the overall absorption. If confirmed by experiment, this may bode well for eventual utilization of EMNs in increasing PV performance.

The optical enhancement afforded by the EMN of Fig. 1(a) is perhaps better seen by plotting the absorption enhancement factor $A(\text{EMN})/A(a\text{-Si})$, that is, the simulated absorption of the EMN structure relative to that in the same thickness $a\text{-Si}$ without the EMN. We show this in Figure 2, where the enhancement factor varies from ~10% improvement at 500 nm to over 1,000% improvement at 700 nm. Again, at this point, these simulations do not inform as to into where the optical energy is being absorbed, other than the “structure” presented in Fig. 1. Further simulations and experiments will eventually provide insight into this question. Nonetheless, this magnitude absorption increase is significant, given that at these lower energies/longer wavelengths, the majority of the metals depicted are highly reflecting (in bulk), rather than absorbing.

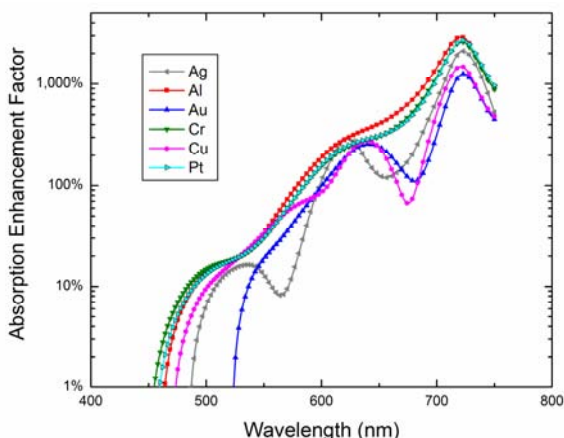


Figure 2. Optical absorption enhancement factor $A(\text{EMN})/A(a\text{-Si})$ calculated from simulation data of alternating square EMN in Figure 1, showing over significant (>1,000%) enhancement for long wavelengths, for all metals employed.

2.2 Cross EMN on ITO-Glass

The second EMN pattern simulated was an array of subwavelength crosses, as depicted in Figure 3. A square unit cell with 630 nm sides contained a symmetric cross with 200 x 500 nm arms 35 nm thick. An array of this EMN was embedded 45 nm below the surface of an 80 nm-thick $a\text{-Si}$ film, similar to the EMN in Fig. 1(a). In addition, the inner and outer corners of this EMN structure were intentionally rounded, with a radius of curvature of 50 nm, to more closely approximate what we have been able to fabricate and test experimentally, as shown later. The simulated absorption for this structure is shown in Fig. 3(b), along with a control simulation for the same film stack but without the EMN. Similarly to Fig. 1, inclusion of the EMN enhances absorption, in the present case by more than 40% integrated across the 400 – 750 nm wavelength regime. The absolute value of the absorption is somewhat less than the case of the alternating square pattern, however.

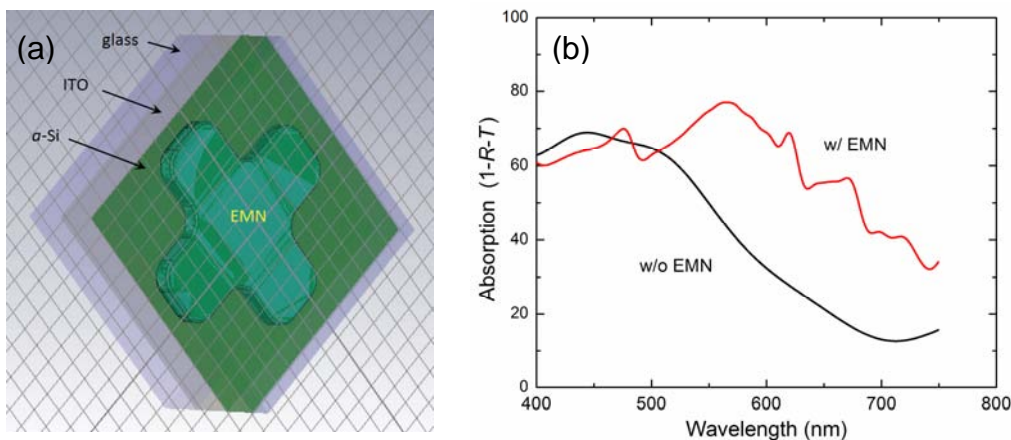


Figure 3. (a) Cross-shaped EMN in $a\text{-Si}$, positioned on ITO-glass, as in Fig. 1. (b) Simulated optical absorbance for the structure in (a) with and without the embedded metal nanopattern.

2.3 Alternating Square EMN on Metal

In addition to simulating optical absorbance in the stack configuration of Figure 1 and 2, we performed simulations of the same EMN patterns arranged within a silicon film on a metallic (Ag) substrate. This differs from the prior configuration in that the Ag film can act as a back-reflector, giving incident light up to two passes through the Si/EMN medium. The configuration is shown in the inset to Figure 3: a 40 nm total thickness *a*-Si film is placed on a 50 nm-thick Ag film, with a 20 nm-thick alternating square EMN (with same lateral dimensions as Fig. 1) embedded at various depths *d* below the top *a*-Si surface. Here, *d* = 0 refers to the top edge of the EMN being flush with the top edge of the silicon. Rather strong absorption ($A > 90\%$) results for wavelengths above 600 nm for this case, with this long-wavelength absorption diminishing as the EMN depth (*d*) increases. Meanwhile, once the EMN is fully buried (*i.e.* $d > 0$), high energy/short wavelength light absorption notably increases, to over 90%. This may be attributed to the fact that the electric field intensity is enhanced near all surfaces of the EMN, including the top surface facing the incident light.

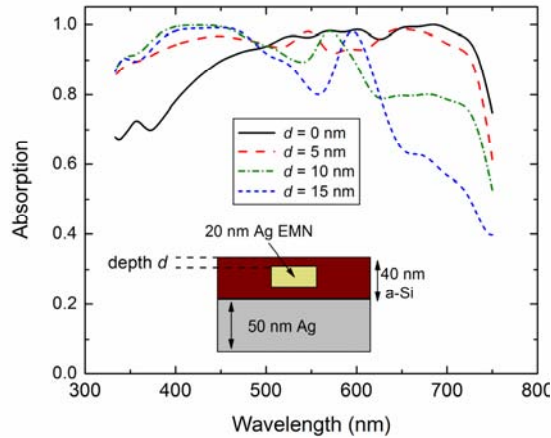


Figure 4. Simulations of optical absorbance for alternating square EMN of Fig. 1 dimensions on Ag substrate, as shown in inset, for various depths *d* as indicated.

2.4 Cross EMN on Metal

Finally, we show in Figure 5 the cross-pattern EMN of Fig. 2 in the metal-backed configuration of Fig. 4, for two EMN depths, $d = 0$ and $d = -20$ nm (*i.e.* for the metal nanopattern situated on top of the Si film, rather than embedded). This figure serves to demonstrate the potential advantage of embedded subwavelength nanostructures fully within the semiconductor absorber layer, as opposed to merely placing it on top. Absorbance between 80% and 95% is simulated/predicted for a mere 40 nm thick *a*-Si film, with integrated absorption (over the wavelength range shown) for the embedded case ($d = -5$ nm) more than 60% larger than for the surface case ($d = -20$ nm).

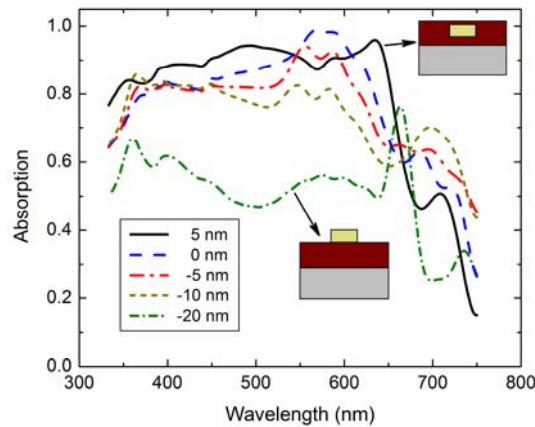


Figure 5. Simulations of optical absorbance for cross pattern EMN with dimensions of Fig. 2, on Ag substrate, as shown in inset, for various depths *d* as indicated. The two extreme situations are sketched.

3. EXPERIMENTS

Test substrates were fabricated using commercial 0.7 mm thick glass substrates coated with 500 nm ITO, diced into 1 cm x 2 cm coupons. Amorphous Si was deposited by PECVD. The thickness of an initial *a*-Si layer depended on the distance the metal layer was to be embedded into the *a*-Si layer (including zero). The sample was removed from the PECVD chamber, and the metal pattern created by standard e-beam lithographic techniques. Two layers of PMMA were coated onto the ITO glass wafer. The first layer was PMMA 495 A4, spin coated for 60 s at 4000 rpm and hard baked for 20 min at 180 C; the second layer was PMMA 950 A4.5, spin coated for 60 s at 5000 rpm and hard baked for 20 min at 180 C. E-beam writing was done in the JEOL 7001 SEM system integrated with a Nabity nanometer pattern generation system e-beam writing code. The sample was then put back into the PECVD chamber and the *a*-Si deposition resumed. As the area of the metal pattern was small, 2 mm x 2 mm, compared to the coupon, the non-metalized areas served as optical measurement controls for areas with the nanopatterned embedded metal.

In Figure 6 we show one such e-beam lithographed cross test pattern composed of 100 e-beam exposure fields, each 120 μm on edge, stitched together to form a 1.2 mm x 1.2 mm test pattern. At the finest scale (lower right), the crosses deviate from the ideal crosses in that the corners show some rounding. The dimensions of this EMN are indicated.

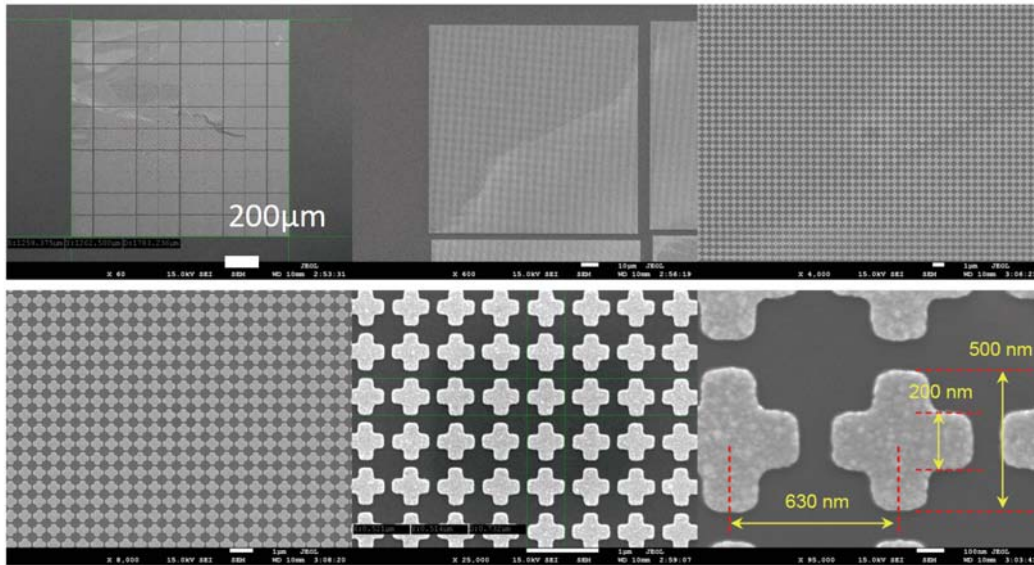


Figure 6. 1 mm x 1 mm e-beam lithographed cross pattern as fabricated, designed to mimic the EMN simulated above.

Optical measurements, both reflection and transmission, were performed using a modified fiber optic spectrometer from Ocean Optics which measures the 0th order reflection R_0 and transmission T_0 of small sample areas ($< 200 \mu\text{m}$ diameter). The apparatus consisted of a bifurcated optical fiber, of which one arm was connected to the spectrometer and the other to a light source for reflectance measurements as shown in Figure 7. For a reflectance measurement, the reflection source is lit, and spectra are taken of a front surfaced silver reference mirror which acts as the 100% reflecting standard, then the mirror is replaced by the sample. The sample spectra are normalized by the silver mirror spectra, thus producing a sample reflectance spectra that ranges from 0 to 100% reflectivity (as compared to the Ag reference).

For transmission measurements, the transmission source is lit and spectra are taken of a reference substrate without the films/structures of interest, and then a spectrum of the sample of interest. The sample spectra is normalized by the transparent substrate spectra, thus producing a sample transmission spectra that ranges from 0 to 100% transmission (as compared to the bare substrate). From these two measurements, the 0th order absorbance (A_0) can be calculated as $A_0 = 1 - R_0 - T_0$.

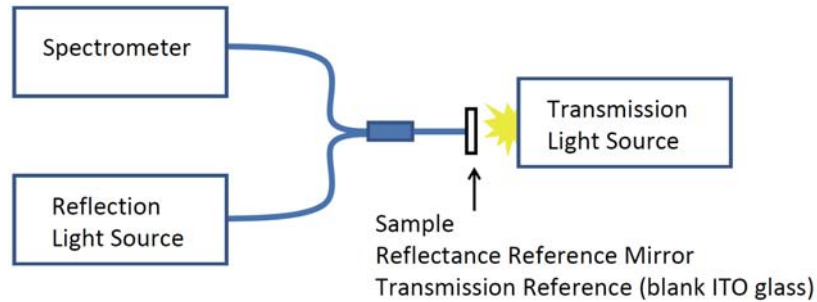


Figure 7. Apparatus for measuring 0th order reflection and transmission of small area samples. Fiber is placed against sample over area to be measured.

4. EXPERIMENTAL RESULTS

Based on measurements of the 0th order transmission and reflection of an 80 nm thick *a*-Si film on ITO coated glass, in Figure 8 we show experimental results for absorbance with and without the EMN shown in Figure 6. As one can see, there is general agreement with the aforementioned simulations showing that the EMN enhances the absorption, particularly at longer wavelengths. At ~660 nm, for example, the absorption in the EMN sample is 3.5 times that of the sample without the EMN, while the total wavelength-integrated enhancement is by more than 50%. This initial result is in good qualitative agreement with the simulations for a similar EMN structure in Fig. 3 above.

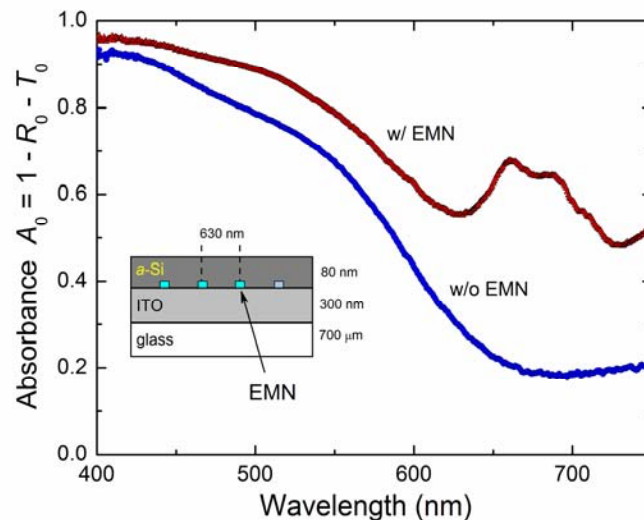


Figure 8. Experimental 0th-order absorbance for the sample described in the text. Note the enhancement of long wavelength absorption in this sample, comprised of subwavelength-dimensioned Ag crosses (Fig. 6).

5. CONCLUSIONS

We have simulated optical absorbance spectra for two metal nanopatterns, consisting of arrays of alternating squares and crosses with subwavelength dimensions and pitch, embedded in thin amorphous silicon films. We find considerable enhancements (up to 3,000%) in absorption, particularly at red to infrared wavelengths. The degree of enhancement depends on the metal material chosen, the pattern structure and, in particular, the embedded depth in the silicon. We have also fabricated a silver EMN structure in *a*-Si and measured the optical reflectance and transmittance, from which the absorbance spectrum is obtained. In comparison to an identical film stack but without the EMN, we find more than 50% increased absorption integrated across the visible, with a maximum enhancement of ~250% near 680 nm. Encapsulating such metal EMN structures in an insulating coating should eliminate concerns about their functioning as electron-hole recombination surfaces, and enable their incorporation into ultrathin film photovoltaic solar cells having anomalously strong optical absorption.

REFERENCES

- [1] Atwater, H.A. and Polman A., “Plasmonics for improved photovoltaic devices”, *Nature Mater.* **9**, 205-213 (2010).
- [2] Chen, H., Chan, C. and Sheng, P. “Transformation optics and metamaterials”, *Nature Mater.* **9**, 387-396 (2010).
- [3] Derkaacs, D., Lim, S. H., Matheu, P., Mar, W., Yu, E. T., “Improved performance of amorphous silicon solar cells via scattering from surface plasmon polaritons in nearby metallic nanoparticles”, *Appl. Phys. Lett.* **89**, 093103 (2006).
- [4] Qu, D., Liu, F., Yu, J., Xie, W., Xu, Q., Li, X., Huang, Y., “Plasmonic core-shell gold nanoparticle enhanced optical absorption in photovoltaic devices”, *Appl. Phys. Lett.* **98**, 113119 (2011).
- [5] Schaadt, D. M., Feng, B., Yu, E. T., “Enhanced semiconductor optical absorption via surface plasmon excitation in metal nanoparticles”, *Appl. Phys. Lett.* **86**, 063106 (2005).
- [6] Moulin, E., Sukmanowski, J., Luo, P., Carius, R., Royer, F.X., Stiebig, H., “Improved light absorption in thin-film silicon solar cells by integration of silver nanoparticles”, *J. Non-Cryst. Sol.* **354**, 2488-2491 (2008).
- [7] Eminian, C., Haug, F.-J., Cubero, O., Niquille, X., Ballif, C., “Photocurrent enhancement in thin film amorphous silicon solar cells with silver nanoparticles”, *Prog. Photovolt: Res. Appl.* **19**, 260-265 (2011).
- [8] Nagel J. R. and Scarpulla, M. A., “Enhanced absorption in optically thin solar cells by scattering from embedded dielectric nanoparticles”, *Opt. Exp.* **18**, A139-A146 (2010).
- [9] Rand, B.P., Peumans, P., Forrest, S.R., “Long-range absorption enhancement in organic tandem thin-film solar cells containing silver nanoclusters”, *J. Appl. Phys.* **96**, 7519-7526 (2004).
- [10] Palik, E.D. Editor, [Handbook of optical constants of solids], Academic, New York (1998).
- [11] Bass, M., [Hand Book of Optics, Vol. II], McGraw-Hill, New York (1995).